Electronic conduction in the layered semiconductor $MnPS_3$

1989 J. Phys.: Condens. Matter 1 3337

(http://iopscience.iop.org/0953-8984/1/21/004)

J. Phys.: Condens. Matter **1** (1989) 3337–3347. Printed in the UK

Electronic conduction in the layered semiconductor $MnPS_3$

V Grasso†, F Neri†, S Santangelo†‡, L Silipigni† and M Piacentini§

† Istituto di Struttura della Materia, Università degli Studi di Messina, Salita Sperone 31, PO Box 57, I-98166 S Agata Messina, Italy

§ Dipartimento di Energetica, Università degli di Roma I, 'La Sapienza', I-00185 Roma, Italy

Received 4 August 1988, in final form 24 October 1988

Abstract. Thermopower, conductivity and photoconductivity measurements as a function of temperature, from 130 to 320 °C, have been carried out on manganese thiophosphate, $MnPS_3$. The transport mechanisms involved in distinct temperature ranges and under different illumination conditions have been identified. At 130 °C a dark conductivity value of 8.6×10^{-13} Ω^{-1} cm^{-1} has been measured, while photoconductivity values ranged from 8.8×10^{-13} to 6.1×10^{-8} Ω^{-1} cm^{-1}. In particular, the dark conductivity process has been attributed to holes in the phosphorus $3p_z$ valence band. The results have been interpreted on the basis of a model, already used for $NiPS_3$, that assumes a weak, ionic, interaction between the transition-metal and the sulphur atoms. A possible energy distribution of both valence and conduction bands, together with Mn 3d levels, is also provided.

1. Introduction

The compound $MnPS_3$ is a layered semiconductor belonging to the transition-metal chalcogenophosphate family, generally indicated as MPX_3 (M stands for transition-metal ion and X is either sulphur or selenium). This class of materials is particularly interesting from both fundamental and technological points of view. In fact, owing to the high structural anisotropy exhibited and to the ability to intercalate alkali-metal ions (e.g. lithium) without any significant parameter expansion, they represent promising candidates for the preparation of low-cost cathodes for high-energy-density batteries (Le Mehauté *et al* 1977, Thompson and Whittingham 1977, Brec *et al* 1978, 1982, Rouxel *et al* 1983). While structural, optical, magnetic and, in part, electrical properties of these materials have been widely investigated (Banda 1986, Foot *et al* 1980, Foot and Nevett 1986, Grasso *et al* 1986a, b, Khumalo and Hughes 1981, Whangbo *et al* 1985, Piacentini *et al* 1982, Brec *et al* 1980, 1985, Taylor *et al* 1973), a detailed study of the electronic states is still lacking. Such a study is essential to understand the origin of the different behaviour presented by each compound upon intercalation.

In a previous paper (Grasso *et al* 1988) we presented a study of the electrical transport properties of $NiPS_3$. We showed that the experimental results were interpreted satisfactorily on the basis of a semi-empirical energy level model proposed by Piacentini *et al* (1982). This model, adopted to explain the characteristic features of optical absorption

‡ Present address: Facoltà di Ingegneria, Università di Reggio Calabria, 89100 Reggio Calabria, Italy.

0953-8984/89/213337 + 11 $02.50

and x-ray photo-emission spectra, was based primarily on a single-layer approximation and on a mainly ionic metal–sulphur bond type, e.g. $M_2^{2+}(P_2S_6)^{4-}$. Because of the striking similarities among MPS_3 compounds, such a model can be used as a starting point for the interpretation of several physical properties related to the energy distribution of the electronic states.

Up to now, no exhaustive study of the electrical transport properties of pure $MnPS_3$ has been reported in the literature, at least to our knowledge. Thus, the temperature dependence of thermopower, photoconductivity and dark conductivity measurements presented in this paper and their interpretation constitute an attempt to determine the conduction mechanisms in relation to the electronic energy band structure of this compound.

2. Experimental details

The samples were grown and provided by R Brec (University of Nantes, France); for details of preparation see Ouvrard (1980). Single crystals of $MnPS_3$, different in size, were selected for thermopower and in-layer conductivity and photoconductivity measurements. The samples were cleaved and mounted on Corning 7059 glass in an inert atmosphere, and then transferred to a cryostat, which allows one to operate from liquid-N_2 temperature up to about 400 °C. The electrical contacts were provided by conducting silver paint, and we checked the linear behaviour of the *I–V* characteristics for the polarisation voltages used. All measurements were performed in a DC configuration at pressures of about 10^{-6} Torr, and were repeated several times, on two samples of different thickness, in order to check for their reproducibility. Dark conductivity measurements showed reproducibility better than 9%, while those for the photoconductivity were better than 30% for infrared (IR) illumination and 16% for all other cases. Particular care was taken to avoid the formation of free surface adsorbates. Owing to the extremely high sample resistance (about 10^{13} Ω at 130 °C), it was not possible to investigate the temperature range below about 130 °C. An HP 3421A data logger, connected to a microcomputer, was used to collect all the data and to calculate the conductivity, photoconductivity and thermopower values in real time.

The dark conductivity and photoconductivity measurements were carried out on a single crystal of $MnPS_3$, approximately $0.048 \times 2.8 \times 1.5$ mm in size, at heating rates less than 1 °C min^{-1} to avoid undesired effects due to thermo-stimulated currents. A Keithley model 616 electrometer with 10^{14} Ω input impedance was used to measure current. The polarisation voltage (about 10 V) was provided by an HP 6115A precision voltage supply. A 75 W xenon arc lamp, with a measured emitted light intensity of about 500 mW cm^{-2}, was employed as the light source in the photoconductivity measurements. Visible (VIS) and IR transmitting filters were used to vary the wavelength of the incident radiation, while the intensity was changed by means of some neutral density filters.

Measurements of Seebeck coefficients (S) were made on a single crystal of $MnPS_3$ about $0.208 \times 4.0 \times 1.2$ mm in size, using a differential method (Grasso *et al* 1988). During the measurements, particular attention was taken to ensure the achievement of thermal equilibrium of the sample holder before acquiring S values.

3. Results

Figures 1 and 2 show the temperature dependence of both dark conductivity σ_d and photoconductivity σ_p, the latter being obtained under different illumination conditions.

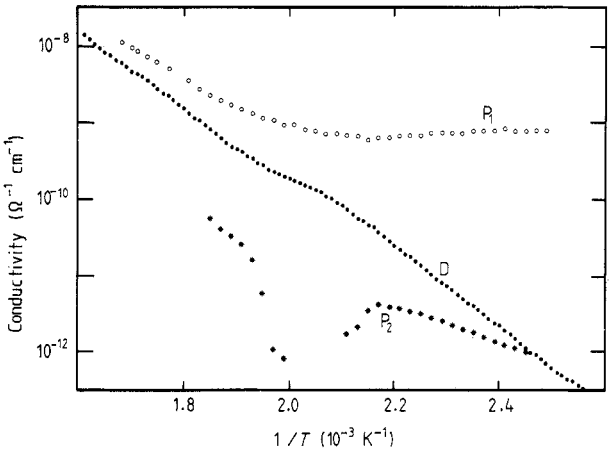

Figure 1. Temperature dependence of in-layer conductivity (curve D) and photo-conductivity (curves P_1 and P_2). P_1 is obtained with a visible transmitting filter, P_2 with a near-infrared (NIR) transmitting one.

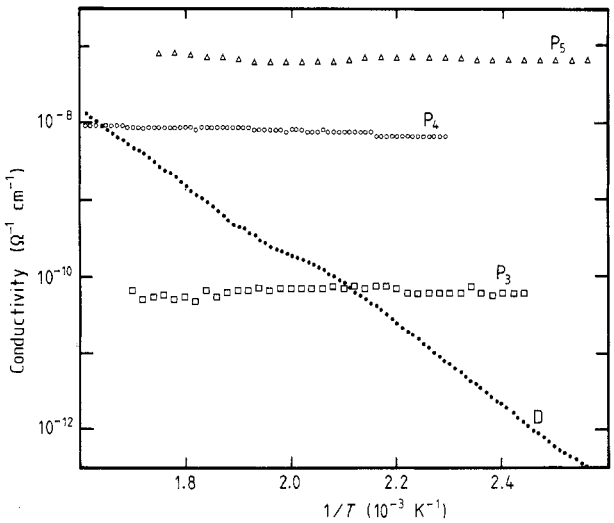

Figure 2. Temperature dependence of in-layer conductivity (curve D) and photo-conductivity (curves P_3, P_4 and P_5). P_3 is obtained with a 0.1% transmitting neutral density filter, P_4 with a 10% transmitting one and P_5 refers to unfiltered light.

The same σ_d curve has been reported on both figures for comparison. Each curve represents an average over several different experimental runs, performed at heating rates less than 1 °C min^{-1}. From the analysis of these results, two different temperature regions can be distinguished: a low-temperature one for $10^3/T$ above 2 K^{-1} and a high-temperature one below this value. As already mentioned, it was not possible to investigate the temperature range below about 130 °C owing to the extremely high resistance of the samples. In all those cases where an activated behaviour was clearly observed, the experimental data were fitted to a relation of the type

$$\sigma = \sigma_0 \exp(-E_a/kT).$$

For each temperature range the pre-exponential factor σ_0 and the activation energy E_a are reported in table 1.

Table 1. Pre-exponential factors σ_0 and activation energies E_a obtained fitting the dark conductivity and photoconductivity experimental curves in two distinct temperature regions (see text).

	High temperature		Low temperature	
	$\sigma_0\,(\Omega^{-1}\,cm^{-1})$	E_a (eV)	$\sigma_0\,(\Omega^{-1}\,cm^{-1})$	E_a (eV)
Photocond. (P_1)	0.01	0.72 ± 0.03	Inactivated	
Photocond. (P_2)	—	—	4.04×10^{-6}	0.54 ± 0.01
Dark cond. (D)	1.67	1.00 ± 0.01	1.38×10^{1}	1.06 ± 0.02

The temperature dependence of σ_p has been investigated varying both the wavelength and the intensity of the incident radiation. The P_1 and P_2 curves of figure 1 have been obtained with a VIS transmitting filter (photon energies ranging from 1.75 to 4.3 eV) and with an IR transmitting filter (photon energies lower than 1.75 eV), respectively. Except for the IR illumination, in which a few seconds were necessary, in all other cases, on switching off the light, the photoconductivity reverts to its dark value almost instantaneously. Curve P_1 is activated only in the high-temperature range, while curve P_2 is activated in the low-temperature region (see table 1 for the activation energy values). In addition curve P_2 shows an odd behaviour around 230 °C: σ_p tends to decrease with increasing temperature, reaching nearly zero values in that interval where no experimental points are reported. This means that $\sigma_i \simeq \sigma_d$, σ_p being defined as the difference between the conductivity under illumination σ_i and that in the dark. Owing to experimental limitations it was not possible to extend the measurements through all the high-temperature region.

Curves P_3, P_4 and P_5 of figure 2 have been obtained with the light from the xenon lamp filtered by some neutral density filters: P_4 with a 10% transmitting filter, P_3 with a 0.1% transmitting one, while P_5 refers to unfiltered light. The photon energies are lower than 5.2 eV, being limited only by the transmission of the cryostat quartz window. All the curves show an activated behaviour through the investigated temperature range, despite a σ_p variation of more than three orders of magnitude between them.

The temperature dependence of the Seebeck coefficient S is reported in figure 3. Owing to experimental limitations involving both the high sample resistance, which limits the low-temperature measurements, and the thermal losses, which limit the sample holder thermal equilibrium at high temperatures, thermopower experimental data could be collected only over a temperature range narrower than that of the conductivity measurements. These reasons explain the spread of the data and the relatively large error bars. Nevertheless the data are found to be almost linear in $1/T$ and the positive sign of S indicates that $MnPS_3$ behaves as a p-type semiconductor. For a crystalline non-degenerate semiconductor with current carriers of only one type, which is appropriate in this case, the thermopower can be expressed as

$$S = S_0 + E_s/kT \qquad \text{where} \qquad S_0 = kA/q$$

and k denotes Boltzmann's constant, q the charge carrier, E_s the energy difference between the Fermi level and the conduction path level and AkT the average energy of the transported carriers relative to the band edge.

The experimental data were fitted to the above formula with a least-squares algorithm which takes into account the uncertainties affecting both S and T (Krane and Schecter

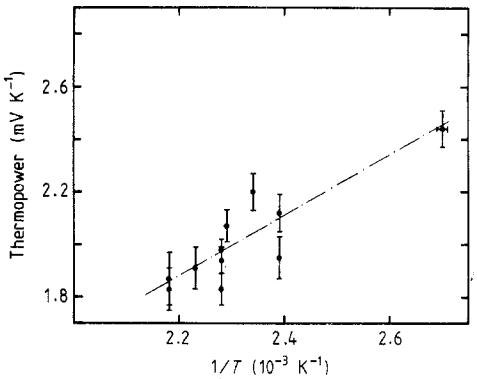

Figure 3. Temperature dependence of thermopower in manganese thiophosphate. The full circles and the chain line represent the experimental data and the best fit, respectively.

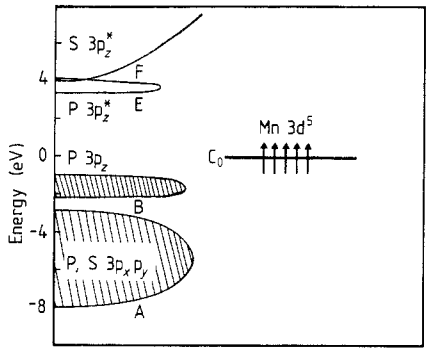

Figure 4. Simplified version of the energy level scheme adopted to describe the electronic band structure of $MnPS_3$. A and B denote the valence bands arising from the $3p_xp_y$ hybridisation of P and S, and from the $3p_z$ bonding orbitals of P–P, respectively. E and F represent the lowest conduction states consisting of $3p_z^*$ antibonding orbitals of S and P. C_0 denotes the ground-state energy of the Mn^{2+} d electrons in the crystal. The energy values are referred to the Fermi energy level, which is assumed to coincide with the C_0 level (see text).

Table 2. Activation energy E_s and S_0 values obtained by fitting the low-temperature thermoelectric power data. The difference between the dark conductivity and the thermopower activation energy is also indicated.

E_s (eV)	S_0 (mV K^{-1})	$E_s - E_d$ (eV)
1.16 ± 0.16	−0.67 ± 0.37	0.16

1982). The calculated E_s value, reported in table 2, coincides, within the estimated error, with the value of the dark conductivity activation energy E_a reported in table 1.

4. Discussion

4.1. Model

As already mentioned in the introduction, several experimental studies have been carried out on transition-metal thiophosphates, mainly regarding their structural, optical and electronic properties. Nevertheless, only in very few cases (Foot *et al* 1980, 1986) have the conduction processes been investigated, probably as a consequence of lack of an appropriate theoretical band structure model. In fact the complexity inherent in the monoclinic unit cell of MPS_3, which contains four $M_2P_2S_6$ molecules each contributing 48 electrons to filling the crystal energy bands, is the reason for making the fundamental simplification of assuming, in turn, the phosphorus atom (Whangbo *et al* 1985) or the transition-metal atom (Piacentini *et al* 1982) as weakly interacting with the sulphur atoms.

The so-called M weakly interacting model (Piacentini *et al* 1982), where M stands for transition metal, seems to work better in explaining the features of soft x-ray valence-band spectra and of below-band-gap optical absorption spectra. Moreover, with such a model we have successfully explained, in a previous paper, some electrical transport properties of $NiPS_3$ (Grasso *et al* 1988). For these reasons we will adopt the same model also in this case. With respect to the nickel compound, a semi-empirical energy level calculation is lacking in this case, so we will use the Ni energy level scheme only as a guide, i.e. we hypothesise that the arrangement of electronic states is the same, with differences only in the energy separations between the levels. Such an assumption is justified in this model, from the fact that the transition-metal 3d levels play no significant role in bonding, and so are viewed as localised, while $P_2S_6^{4-}$ cluster orbitals are the origin of the valence and conduction band states. Thus changing the transition-metal atom would presumably not alter the overall arrangement of electronic levels. The proposed simplified version of the energy level scheme is shown in figure 4. In an octahedral chalcogen surrounding, the single-electron d states split into t_{2g} and e_g sublevels. The d^5 high-spin ground-state configuration of Mn^{2+} is the spin-up $(t_{2g})^3$ $(e_g)^2$ configuration (Ballhausen 1962) corresponding to a $^6A_{1g}$ state. We will not consider the d-level substructure as relevant for our discussion. Also we will not be interested in the possible modifications of the overall Mn^{2+} d-electron configuration because of the excitation of electrons from other electronic states. In the following we will simply identify by C_0 the Mn^{2+} d^5 state (partially filled d level) and by C_1, C_2 and C_3 some of its excited states. A and B will denote the valence bands arising from the $3p_xp_y$ hybridisation of P and S atomic orbitals and from the $3p_z$ bonding orbitals of the P–P pair, respectively. E and F will represent the lowest conduction states consisting of $3p_z^*$ antibonding orbitals of S and P.

The above simplified scheme, reported in figure 4, will be used to interpret the thermopower, dark conductivity and photoconductivity data.

4.2. Thermopower

The temperature dependence of the thermo-electric power S can yield useful information on the transport properties because it is a far more sensitive experimental approach than measurement of conductivity. In particular, a plot of S versus $1/T$ yields the energy difference E_s between the Fermi level and the predominant current path, while its sign will reflect the predominant carrier type. With reference to the energy level scheme of figure 4, as the sign is positive with an activation energy of 1.16 ± 0.16 eV and the Fermi level is located on the C_0 state, we suggest that the conduction process is due to holes and takes place in the valence band originating from the phosphorus $3p_z$ states. In addition, the relatively high Seebeck coefficient values of the order of 2 mV K^{-1} tend to exclude the possibility of ambipolar conduction. That holes are the dominant carriers can also be deduced from the consideration that, as the C_0 level is treated as a localised state in our energy level model, the electron contribution to conduction will certainly be lower than that of any other carrier moving in extended band states. This conclusion is at variance with that of Byvik *et al* (1982); nevertheless the experimental techniques adopted are completely different and the authors themselves stressed the fact that $MnPS_3$ samples were very unstable in both acid and base solutions of their photo-electrochemical cells. As a final consideration we observe that we have found $MnPS_3$ to be a p-type semiconductor just like $NiPS_3$, and this is very plausible, having attributed the same band structure to both materials.

From the above considerations we can draw the conclusion that thermopower measurements locate the P $3p_z$ band about 1 eV lower than the partly filled Mn d level.

4.3. Dark conductivity

It must first be pointed out that, to our knowledge, there are no other electrical transport data on pure $MnPS_3$, so we will base the discussion only on the present results.

The conductivity activation energy value, calculated in the low-temperature range and reported in table 1, is in good agreement with that deduced from thermopower measurements. Thus the same conduction mechanism, i.e. by holes in the valence $3p_z$ band, is to be envisaged. Two other considerations support this conclusion.

(i) From the dark conductivity pre-exponential value reported in table 1, it is possible to give an estimation of the carrier mobility μ, using the relation $\sigma_0 = e\mu N_0$ and assuming $N_0 = 2.51 \times 10^{19}$ cm^{-3}, which is a typical value for the parabolic band approximation. The calculation gives $\mu = 4$ cm^2 V^{-1} s^{-1}, which is a reasonable value for an extended band conduction mechanism and compares well with the corresponding values in other high-resistance layered compounds (Fivaz and Schmid 1976).

(ii) Although it is not reported in this paper, we have calculated and plotted against $1/T$ the quantity Q, given by the relation

$$Q = \ln \sigma + Sq/k.$$

Within experimental error, Q-values are nearly constant as a function of temperature. As is well known (Beyer 1984), Q is independent of any statistical shift of the Fermi level and of temperature-induced shifts of band-gap, and thus thermopower and conductivity data are reciprocally consistent, reinforcing the hypothesis of a single conduction path in valence band states.

Looking at the high-temperature behaviour of σ_d, it can be noted from figure 1 that, before again taking up an activated trend with similar activation energy value (see table 1), a sort of kink is observed around 2×10^{-3} K^{-1}. Two effects could produce such a discontinuity in σ_d, namely a variation in hole mobility or in the distribution of the density of states. The first seems to be unlikely; the latter could be possible if we consider the presence of a very fine substructure in the Mn d states. Effectively the presence of such a fine splitting, of the order of 0.1 eV, has been proposed in the literature (Piacentini *et al* 1982) for t_{2g} levels of $NiPS_3$ and ascribed to a trigonal field effect due to a not well matching value of β, the monoclinic unit-cell angle. Because $MnPS_3$ also presents a not ideal β value (Brec *et al* 1980, Taylor *et al* 1973) this could be a tentative explanation for the observed kink in σ_d.

4.4. Photoconductivity

For sake of clarity we have reproduced in figure 5 the energy level diagram of figure 4 with the different excitation processes and we have also added the excited states of the d^5 electronic configuration indicated by C_1, C_2 and C_3. Their position, relative to the ground state C_0, has been obtained from optical spectra (Grasso *et al* 1986b), where several absorption features belong to d–d intra-configurational transitions are present. With reference to figures 1 and 2, we have identified three principal processes of excitation and recombination, which are discussed in the following.

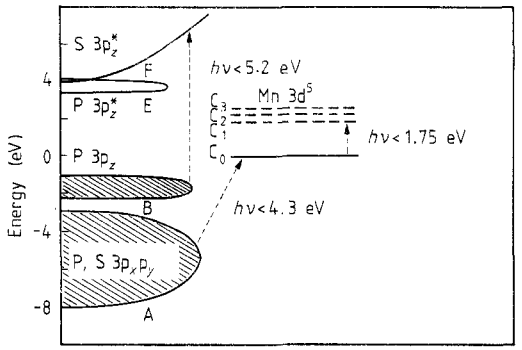

Figure 5. Simplified version of the energy level scheme adopted to describe the electronic band structure of $MnPS_3$. The nomenclature is the same as that of figure 4. C_1, C_2 and C_3 denote the excited states of the Mn^{2+} d^5 electronic configuration (broken horizontal lines). In addition the three different light excitation processes (see text) are also shown. The energy values are referred to the Fermi energy level, which is assumed to coincide with the C_0 level (see text).

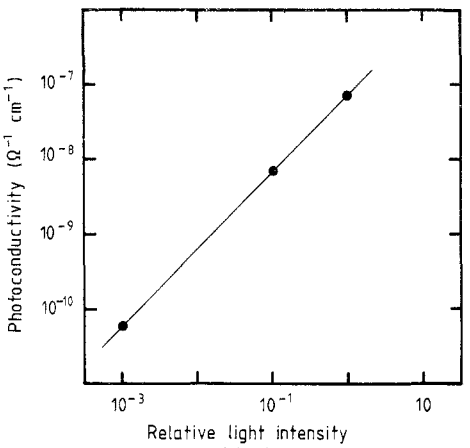

Figure 6. Logarithmic plot of the photoconductivity σ_p dependence upon the relative light intensity I. The experimental values are obtained from P_3, P_4 and P_5 of figure 2.

4.4.1. NIR light: $h\nu < 1.75$ eV. Electrons are excited from C_0 to C_1 (first d–d transition observed in optical spectra), while the recombination path is through level C_0 and band B (see diagram). In equilibrium conditions

$$f = Kp_v n_0'$$

where f is the generation rate, p_v the hole concentration in valence band B and n_0' the electron concentration in level C_0. At thermal equilibrium, the following relations hold for the various population concentrations:

$$n_0' = N_0' \exp\left(-\frac{E_0 - E_v}{kT}\right) \qquad n_1 = n_0 \exp\left(\frac{E_1 - E_0}{kT}\right)$$

where n_1 is the electron concentration in C_1, N_0' the concentration of vacant sites in C_0 while E_0, E_1 and E_v represent the energy positions of levels C_0, C_1 and the top of valence band B. In addition, since electrons are excited from C_0 to C_1 it must be that $N_0' \equiv n_1$, and so developing the formulae we obtain

$$n_0' = n_0 \exp\left(\frac{E_1 - E_0}{kT}\right) \exp\left(-\frac{E_0 - E_v}{kT}\right)$$

$$p_v = \frac{f}{Kn_0} \exp\left(\frac{(E_0 - E_v) - (E_1 - E_0)}{kT}\right).$$

Since $\sigma = ep_v\mu$ the last relation predicts an activated photoconductivity behaviour. Substituting for $E_0 - E_v$ the dark conductivity activation energy value and for $E_1 - E_0$ the exciting radiation maximum energy value, i.e. 1.75 eV, we obtain a value of 0.69 eV

for the photoconductivity activation energy. Such a value compares well with the 0.54 eV value experimentally obtained from curve P_2 of figure 1 (see table 1).

Looking at the same figure, but at higher temperatures, it is possible to observe around $2 \times 10^{-3}\,K^{-1}$ a sharp decrease in σ_p, which extends over some tenths of $1000/T$, and a similar retrieval of normal values. It is worth noticing that it happens in the same temperature region where a kink is observed in σ_d and is completely absent in all the other photoconductivity curves. This means that the effect is present only when the C_0 level is directly involved in the conduction process. If we hypothesise, as in the σ_d case, the existence of a substructure in the C_0 level, a tentative explanation can be provided. As is evident from the above formulae, σ_p is directly related to N_0', the vacant-sites concentration in C_0, so on increasing the temperature it happens that the Fermi-level distribution function crosses a forbidden energy state region causing a decrease in N_0' (and consequently in σ_p). With a further temperature increase, an allowed energy state region is crossed, so σ_p recovers normal values. Obviously the phenomenon is much more dramatic in σ_p than in σ_d because the first is a differential effect. Such an explanation is strictly related to the presence of substructure in the d^5 transition-metal level, as outlined in the dark conductivity discussion (§ 4.3). Evidence for a similar situation is reported in the literature for $NiPS_3$ (Piacentini *et al* 1982). In addition some algebraic calculations can be done to estimate the relative splitting of such a sublevel. If we consider the temperatures limiting the anomalous σ_p region, i.e. 180 and 245 °C, and taking as reference the energy position of level C_0 with respect to valence band B, i.e. 1.06 eV, we can estimate the above-mentioned splitting value by requiring that the Fermi distribution functions at the two limiting values are nearly equal (in order to give approximately equal σ_p values). This simple calculation gives $\Delta E_0 = 0.10$ eV, a value similar to that proposed in the literature for $NiPS_3$ (Piacentini *et al* 1982) and obtained from a completely different kind of experimental measurement.

4.4.2. Visible light: $h\nu < 4.3$ eV. The main excitation process is for electrons from band A to level C_0, i.e. the fundamental absorption observed in optical spectra around 3 eV (Grasso *et al* 1986b). In fact, like in $NiPS_3$, symmetry considerations prohibit first- and second-order transitions from P $3p_z$ (band B) to Mn d^5 levels (Grasso *et al* 1988). The incident radiation causes the generation of free holes in band A and of electrons in level C_0. The occupied (unoccupied) 'centres' in band B behave as hole (electron) recombination centres of density n_r (p_r). We will consider two limiting cases.

(i) *Low light $\sigma_p \leqslant \sigma_d$.* As is well known (Rose 1978) the density of excited carriers c is proportional to the carrier lifetime τ_c:

$$c = f\tau_c \qquad \text{and} \qquad \tau_c = 1/vc_r s_c$$

where v, c_r and s_c are the thermal velocity, the recombination-centres density and the capture cross section for the given carrier, respectively.

In the present case, since the recombination centres belong to band B, then $p_r \ll n_r$; furthermore, their nature being identical (as in the $NiPS_3$ case), $s_n = s_p = s$. Hence $\tau_n \gg \tau_p$ and the process with smaller associated lifetime is the one to be seen in photoconductivity, having assumed for simplicity that the thermal velocities v of both carriers are equal. The observed activation energy (in the high-temperature range of σ_p versus $10^3/T$ curve P_1 in figure 1) represents the energy separation between A band top and B band bottom. Thus we can estimate an energy separation between P $3p_z$ and P, S $3p_x p_y$ bands of about 0.72 eV.

(ii) *High light $\sigma_p > \sigma_d$.* In this case it can be demonstrated that (Rose 1978)

$$\tau_n = \tau_p = 2/N_r vs$$

where N_r is the total density of recombination centres (temperature-independent) and we have considered, as above, that $s_n = s_p = s$. Hence, $\sigma_p(T) = \text{const.}$, as observed in the low-temperature range of curve P_1 in figure 1.

4.4.3. UV light: $h\nu < 5.2$ eV. If we refer to the energy level diagram proposed by Piacentini *et al* (1982) some considerations on the symmetry character of the energy levels involved can be drawn. In fact, owing to symmetry selection rules, transitions between P $3p_z$ A_{1g} (B band) and P $3p_z^*$ A_{1u} (E band) are forbidden at first order (Englman 1972); therefore the optical absorption around 5 eV is to be attributed to transitions whose final state is S $3p_z^*$ $A_{1g}A_{2u}$ (F band). Also in this case we will consider two limiting situations:

(i) *Low light $\sigma_p \leqslant \sigma_d$.* As free-carrier densities (holes in band B and electrons in band F) are small compared with recombination-centre densities, the occupancy of the recombination centres is substantially the same after illumination as it was in the dark. Therefore both n_r and p_r are practically constant and, except for the slow dependence of thermal velocity on temperature, the lifetimes (and so σ_p) should be insensitive to temperature if the capture cross sections are temperature-insensitive (high-temperature range of σ_p versus $10^3/T$ curves in figure 2).

(ii) *High light $\sigma_p > \sigma_d$.* The same conditions stated for high light in § 4.4.2(ii) hold in this case, hence $\sigma_p(T) = \text{const.}$ as observed in the low-temperature range of figure 2.

It is interesting to note that the temperature inactivated behaviour is independent of light intensity. In figure 6 we have plotted on a logarithmic scale σ_p versus I, where I is the relative light intensity, which spans over three orders of magnitude. Fitting the experimental data to a power-law relation such as $\sigma_p \sim I^\gamma$, we have obtained $\gamma = 1.03$, yielding a monomolecular type of recombination as predicted by the relation

$$n = f\tau_n = \frac{f}{p_r vs}.$$

The reasons why we have chosen electrons as photocurrent carriers are explained in the following.

As can be readily noted from figure 1, curve P_1 photocurrent values lie between those of curves P_3 and P_4 of figure 2, the first being obtained with a visible–near-infrared transmitting filter, the latter with some neutral density filters. The corresponding estimated light intensities are 140 mW cm^{-2} for P_1, 0.5 mW cm^{-2} for P_3 and 78 mW cm^{-2} for P_4. To explain the high σ_p values of P_3 and P_4 curves relative to those of curve P_1, we argue that, on increasing light energy to the ultraviolet (UV) region, there is a change in photocurrent carrier type and consequently an increase in photocurrent due to a higher carrier mobility. In fact, as reported in the literature (Fivaz and Schmid 1976), electron mobility for this class of materials is larger than hole mobility, explaining the high σ_p values obtained with relatively low light intensities.

5. Conclusions

From the studies reported and discussed above on the transport properties of the layered semiconductor $MnPS_3$, several conclusions can be drawn.

In spite of the absence of a calculated energy level scheme, like in the $NiPS_3$ case, the simple extension of the transition-metal weakly interacting model to the $MnPS_3$ case seems to explain successfully all the experimental data.

It has been possible to provide a rough estimation of the relative separations among all the energy levels involved in the transport mechanisms. Such separations are reported in figure 4.

The different transport mechanisms, observed both in the dark and under distinct illumination conditions, have been identified as hole conduction in A and B bands, except for the case of UV incident radiation where electron conduction in the F band has been hypothesised.

Further experimental evidence has been found for the existence of a fine substructure of about 0.1 eV in the Mn d t_{2g} sublevel.

References

Ballhausen C J 1962 *Introduction to Ligand Field Theory, McGraw-Hill Series in Advanced Chemistry* (New York: McGraw-Hill)

Banda E J K B 1986 *J. Phys. C: Solid State Phys.* **19** 7329

Beyer W 1984 *J. Non-Cryst. Solids* **66** 1

Brec R, Ouvrard G, Louisy A and Rouxel J 1980 *Ann. Chim. Fr.* **6** 499

Brec R, Ouvrard G, Louisy A, Rouxel J and Le Mehauté A 1982 *Solid State Ion.* **6** 185

Brec R, Ouvrard G and Rouxel J 1985 *Mater. Res. Bull.* **20** 1181

Brec R, Schleich D, Louisy A and Rouxel J 1978 *Ann. Chim. Fr.* **3** 347

Byvik C E, Smith B T and Reichman B 1982 *Solar Energy Mater.* **7** 213

Englman R 1972 *The Jahn–Teller Effect in Molecules and Crystals* (London: Wiley–Interscience) p 302

Fivaz R C and Schmid P E 1976 *Physics and Chemistry of Materials with Layered Structures; Optical and Electrical Properties* vol 4, ed. P A Lee (Dordrecht: Reidel) p 343

Foot P J S, Suradi J and Lee P A 1980 *Mater. Res. Bull.* **15** 189

Foot P J S and Nevett B A 1986 *Phys. Status Solidi* a **93** 283

Grasso V, Neri F, Santangelo S, Silipigni L and Piacentini M 1988 *Phys. Rev.* B **37** 4419

Grasso V, Santangelo S and Piacentini M 1986a *Nuovo Cimento* **8** 263

—— 1986b *Solid State Ion.* **20** 9

Khumalo F S and Hughes H P 1981 *Phys. Rev.* B **23** 5375

Krane K S and Schecter L 1982 *Am. J. Phys.* **50** (1) 82

Le Mehauté A, Ouvrard G, Brec R and Rouxel J 1977 *Mater. Res. Bull.* **12** 1191

Ouvrard G 1980 *Doctoral Thesis* University of Nantes p 13

Piacentini M, Khumalo F S, Olson C G, Anderegg J W and Lynch D W 1982 *Chem. Phys.* **65** 289

Rose A 1978 *Concepts in Photoconductivity and Allied Problems* (New York: Krieger) ch 3

Rouxel J, Molinie P and Top L H 1983 *J. Power Sources* **9** 345

Taylor B, Steger J and Wold A 1973 *J. Solid State Chem.* **7** 461

Thompson A H and Whittingham M S 1977 *Mater. Res. Bull.* **12** 741

Whangbo N H, Brec R, Ouvrard G and Rouxel J 1985 *Inorg. Chem.* **24** 2459